Two mechanisms for the formation of the ferronematic phase studied by dielectric spectroscopy

Neelam Yadav [a], Yuri P. Panarin [a,b], Jagdish K. Vij [a,*], Wanhe Jiang [c], Georg H. Mehl [c]

[a] *Department of Electronic and Electrical Engineering, Trinity College, The University of Dublin, Dublin 2, Ireland*
[b] *Department of Electrical and Electronic Engineering, TU Dublin, Dublin 7, Ireland*
[c] *Department of Chemistry, University of Hull, Hull HU6 7RX, UK*

ABSTRACT

A non-chiral ferroelectric nematic compound with a 1,3-dioxane unit in the mesogenic core called 2,3′,4′,5′-tetrafluoro-[1,1′-biphenyl]-4-yl 2,6-difluoro-4-(5-propyl-1,3-dioxan-2-yl) benzoate (DIO) was studied by dielectric spectroscopy in the frequency range 0.1 Hz–10 MHz over a wide range of temperatures. The compound exhibits three nematic phases on cooling from the isotropic phase, i.e., the ordinary paraelectric nematic N; the intermediate nematic N_X and the ferroelectric N_F phase. The least frequency process is due to the dynamics of ions. The middle frequency relaxation process P_1 is like as observed in other ferronematic compounds and this mode is a continuation of the molecular flip-flop motion in the isotropic phase to the collective dynamics of dipoles which are strongly coupled with the splay fluctuations in nematic phases. In addition to this process, DIO shows an additional collective relaxation process P_2 at higher frequencies both in the N and the N_X phases. This mode originates from the polar/chiral domains of the opposite chirality, these arise from the spontaneous symmetry breaking of achiral mesogens in the N phase. Both collective processes, P_1 and P_2, show soft mode-like characteristic behavior on cooling from the N to the N_X-N_F phase transition temperature and are shown to contribute independently to the formation of the ferronematic N_F phase.

© 2023 The Author(s). Published by Elsevier B.V. This is an open access article under the CC BY license (http://creativecommons.org/licenses/by/4.0/).

1. Introduction

Since the discovery of the liquid crystalline state of matter made initially through studies of the derivatives of cholesterol, the chirality and the polarization properties of liquid crystalline phases arose entirely from the molecular chirality. In this case, at least one of the carbon atoms in the molecule is connected to the four different substituents. However, during the last couple of decades, these features have also been observed in achiral liquid crystal (LC) systems composed of bent-core molecules [1] and the bent bi-mesogens or dimers that exhibit the twist-bend LC phase [2,3,38]. In such systems, achiral molecules can also form "chiral phases", which exhibit optical activity and/or the spontaneous polarization. Finally, a new, long-awaited ferroelectric nematic phase predicted more than a century ago by P. Debye [4] and M. Born [5], was discovered independently by two research groups in 2017 [6,7]. In one of the first publications on the ferroelectric nematics, an extremely large dielectric permittivity of $\sim 10^4$ and a high spontaneous polarization of ~ 4.4 μC cm^{-2} were reported

in the compound, 2,3′,4′,5′-tetrafluoro-[1,1′-biphenyl]-4-yl 2,6-difluoro-4-(5-propyl-1,3-dioxan-2-yl) benzoate abbreviated as (DIO) [6]. This material exhibits three variants of nematic phases, such as the ordinary paraelectric nematic (N), an intermediate unknown nematic (N_X), and a ferroelectric nematic (N_F). These were termed initially as M1, M2 and MP for the N, N_X and $N_{F,}$ phases respectively. From the XRD studies made recently by the Boulder group [8], intermediate N_X (or M2) has been found to be density modulated antiferroelectric, SmZ_A phase with a period of 8.6 nm and it has antiparallel and slightly splayed director distributions. However, Sebastian *et al.* prefer to call it just 'splay nematic, N_S' [9], since it belongs to a class of modulated nematic phases where the periodicity of modulation is one of the characteristics of the material.

The other ferroelectric nematic compound RM734 and its homologues with large molecular dipole moments were synthesized by Mandle et al. [7], studied extensively and reported in the literature. These compounds nevertheless exhibit two distinct nematic mesophases: the ordinary paraelectric N and the unknown N_X separated by a weak first-order transition [10]. Later, Mertelj *et al.* [11] showed that the N_X phase forms a splay modulated structure, N_S, with a period varying from 5 to 10 μm; originating possi-

bly from the wedge-shaped molecules of RM734. They therefore term the N_S as the splay nematic phase [12,13,14]. The N-N_S phase transition resembles ferroelectric to ferro-elastic transition that occurs via flexoelectric coupling [12]. Chen *et al.* [15] gave the first major demonstration of ferroelectricity in the N_X phase of RM734 and they confirmed it to be the N_F phase.

The newly discovered phases display fascinating properties, and these are studied by several research groups with the objective of obtaining better understanding of the origin of ferroelectricity in achiral nematics [16]. Novel nematic-nematic phase transitions have recently been reported in some other compounds. Manabe *et al.* [17] synthesized a compound that shows a direct transition from the isotropic state to the N_F phase while Saha *et al.* reported that their synthesized LC material exhibits multiple ferroelectric nematic phases [18].

We report and discuss results of our investigations of DIO with a focus on the high-temperature nematic phases: N and N_X (SmZ$_A$ or N_S) using high resolution dielectric spectroscopy (DS). DS is a versatile technique for investigating the ferroelectric characteristics of liquid crystals since this technique sensitively probes the dynamics of polar molecules without disturbing its phase structure. While the technique [37] does not yield any direct information for micro/nano structure of the phase, nevertheless some structural details are deduced indirectly from the dielectric spectra. Results obtained using DS complement those from other methods: X-ray diffraction, the second harmonic generation (SHG). The DS as a technique is an excellent probe for studying the molecular dynamics of dipolar molecules and in many ways, it is even superior to the electro-optical technique, since the prevailing structure of the LC medium is not altered or significantly disturbed by the application of a weak probe field. A rearrangement of the molecular orientational ordering and a rotational distribution of the dipoles induced by a weak probe field governs the temperature dependent dielectric response of the LC phase under investigation. Hence, DS is used for investigating properties of ferroelectric nematics [14,19,20]. Nevertheless, a major caution is required in using this technique for the study of ferronematic LCs. In each DS study, the texture of the LC cell must be recorded as the proof of the specific alignment. An alignment in the test cells using bare metal electrodes cannot confirm the validity of a specific alignment.

In the past, we used DS successfully to study different phases of LCs: ferroelectric smectic C (SmC) [21], and the twist grain boundary Smectic A (TGBA) etc. [22], ferrielectric [23,24] and antiferroelectric, the SmC LCs [25], de Vries [26], the bent-core nematics [27,28] and the SmCP [29].

The molecular structure and the phase transition temperatures of DIO are recorded under cooling from the isotropic phase at a rate of 0.2 °C/min using dielectric spectroscopic technique and results of the measurements are given in Fig. 1. DIO was resynthesized by the group of G. H. Mehl (Hull, UK) and it shows phase transition temperatures slightly lower than those reported originally [6]. In general, the transition temperature of a compound depends on

the intermediates used in the synthesis and the rate of cooling/heating of the sample cell.

2. Experiment

The complex dielectric permittivity measurements are made using broadband Alpha high-resolution dielectric analyzer (Novocontrol GmbH, Germany). Commercial cells (EHC ltd, Japan) use substrates that are deposited with low sheet resistance indium tin oxide (ITO) electrodes (10 Ω/□). These are coated with poly-imide (LX-1400, Hitachi-Kasei) alignment layers of ∼20 nm thickness for planar alignment, and use cetyl-trimethyl-ammonium-bromide for obtaining homeotropic alignment. A polyester roll, with a fiber length of 8 mm and roll diameter of 58 mm, respectively, was used for rubbing the two opposite surfaces prior to the polymerization of aligning agents. Each surface rubbing is carried out by a roller at a rotational speed of 600 rpm where the stage speed is kept at 30 mm/sec. Measurements of the dielectric permittivity are made under cooling from the isotropic phase using thin aligned cells, filled with the liquid crystalline sample under investigation. The LC cell is mounted in a heating stage of which the temperature is controlled. Measurements were also made for different cell thicknesses as well as by varying thicknesses of the alignment layers. Results of the measurements agree with each other within the experimental error. Furthermore, dielectric measurements were made for different sheet resistances of ITO. Sheet resistance used in these experiments was 10 Ω/□, the lowest sheet resistance that at present is commercially available. The ITO peak for all temperatures under investigations for cells filled with the liquid crystalline material was found to shift to the frequencies beyond the frequency window of the experiment. Results of the measurements are recorded using a small probe voltage of 0.1 V, and temperature of the cell varied in the steps of 1 °C. Results of the experiment are repeatable and furthermore any decomposition of the material is not observed as confirmed by the technique of Thermo-Gravimetric Analysis (TGA). The temperature of the LC cell is stabilized to within ± 0.02 °C.

3. Results and discussion

Prior to making dielectric measurements, textures of the sample are recorded using polarizing optical microscopy (POM). A specific texture under POM characterizes the type of molecular alignment: homeotropic or planar. Textures shown in Fig. 2a–2b confirm that molecules of DIO are aligned perfectly homeotropically both in the N and the N_X phases. The recorded textures are independent of the rotation of the device mounted in the hot stage. However, in the N_F phase (Fig. 2c), a sandy or a grainy texture with no clear extinction of light is observed. Textures of planar-aligned cells (Fig. 2d–f) display perfect homogeneous alignment of the sample in the three phases under investigation.

The temperature dependencies of the real and the imaginary parts of the complex permittivity in the frequency range of 0.1 Hz–10 MHz are recorded for both homeotropic and planar aligned cells. The observed temperature dependent dielectric loss spectra of the longitudinal $\epsilon_{\parallel}''$ and the transverse $\epsilon_{\perp}''$ components of the complex dielectric permittivity are shown in 3D in Fig. 3 for a cell of 4 μm thickness. Fig. 4 shows the dielectric loss spectra for different temperatures in the four phases: 175 °C (I), 150 °C, 130 °C, 90 °C in N, at 70 °C in the N_X; and at 50 °C in the N_F phase. The spectra are analyzed using WINFIT software, developed by Novocontrol GmbH, Germany. The complex permittivity data are fitted to the Havriliak - Negami (H-N) equation [30], with the conductivity term included in the equation [31,32]:
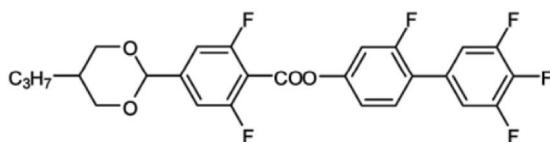
X − MP (N_F) 66.8 M2 (N_X) 83.5 M1 (N) 173.8 Iso (°C)

Fig. 1. The molecular structure, the phase-sequence, and the transition temperatures of DIO. Nomenclature of the phases here is drawn from the works of Nishikawa *et al.* [6] and Chen *et al.* [8].
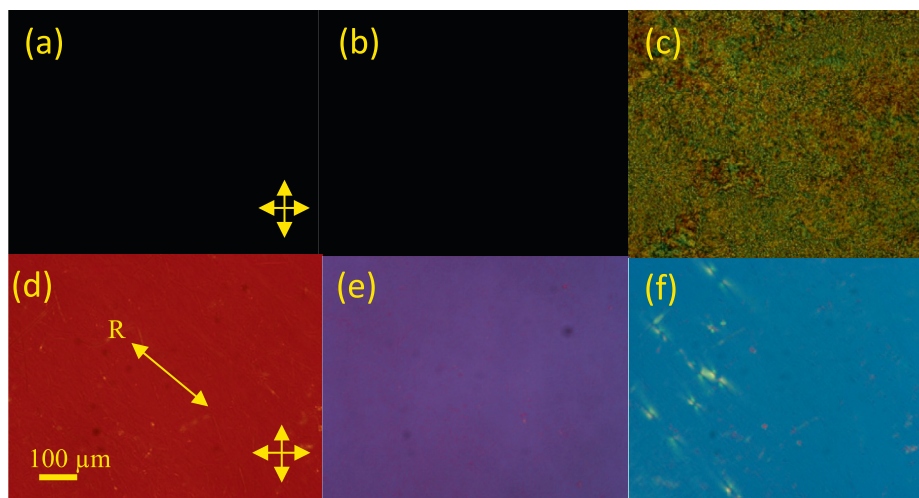
Fig. 2. Textures of DIO recorded in a homeotropic cell at (a) 130 °C (N), (b) 70 °C (N$_X$) (c) 60 °C (N$_F$) and in planar aligned cells of 4 μm thickness (double-headed arrow in 2(d) is the rubbing direction (R) at temperatures (d) 130 °C (N) (e) 70 °C (N$_X$) (f) 60 °C (N$_F$) under crossed polarizers.
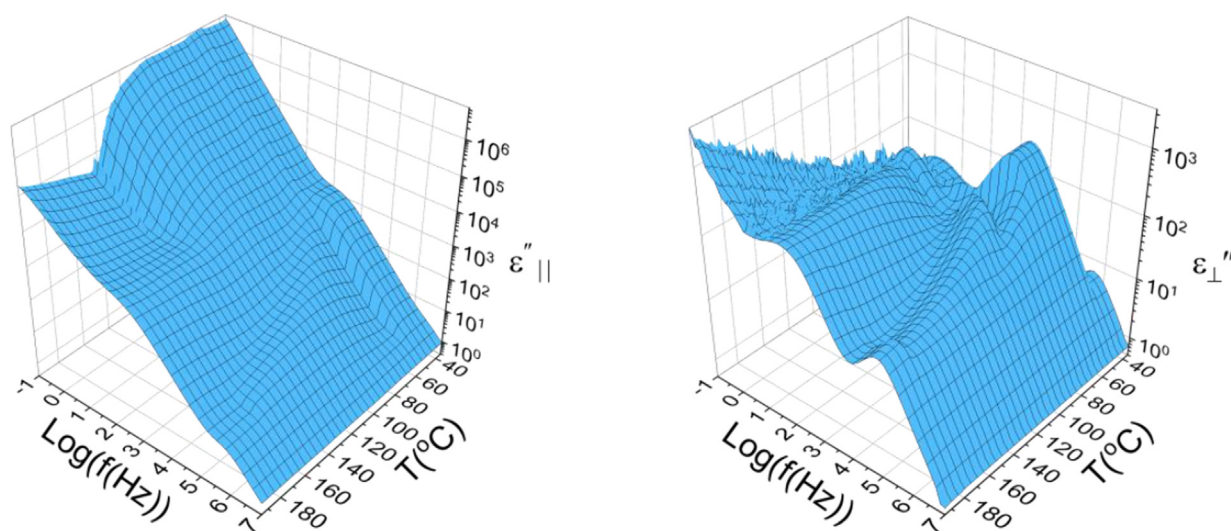
Fig. 3. Three-dimensional (3D) dielectric loss spectra of DIO in a cell of thickness 4 μm (a) homeotropic, and (b) planar homogeneously aligned cell.
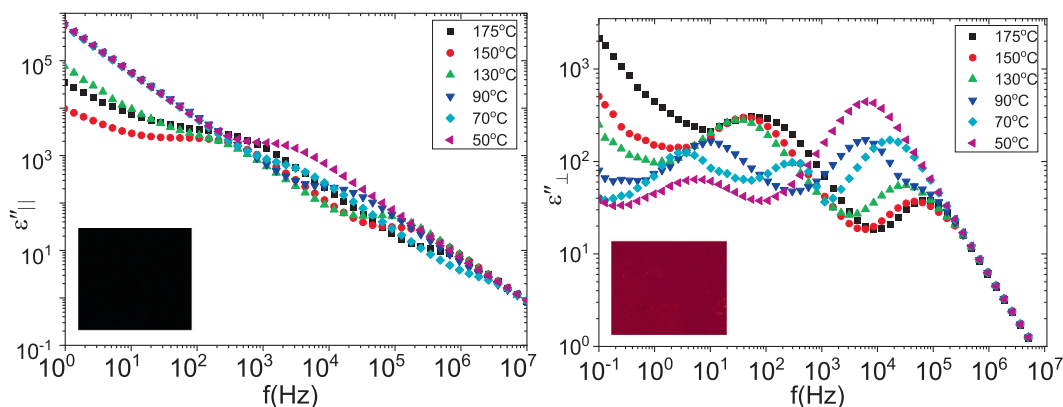
Fig. 4. Two dimensional cuts of the 3D plots of dielectric loss versus frequency (Fig. 3) at different temperatures: 175 °C in the Iso phase and for 150 °C, 130 °C, 90 °C in M1 (N) phase; at 70 °C in M2 (N$_X$); and at 50 °C in MP (N$_F$) phase; **4**(a) homeotropic cell and 4(b) planar aligned cell. The insets in Figures depict texture of aligned DIO sample: homeotropic (a), and the planar aligned (b) both in the nematic (N) phase.

$$\varepsilon^* = \varepsilon_\infty + \sum_{j=1}^{n} \frac{\Delta\varepsilon_j}{\left[1 + \left(i\omega\tau_j\right)^{\alpha_j}\right]^{\beta_j}} - \frac{i\sigma}{\varepsilon_0\omega}, \qquad (1)$$

where ε^* is the complex dielectric permittivity, ε_∞ is the high frequency dielectric permittivity that includes electronic and atomic polarizabilities of the material, ω ($=2\pi f$), is the angular frequency of the probe field, ε_o is the permittivity of free space, σ is the conductivity, τ_j is the relaxation time, $\Delta\varepsilon_j$ is the dielectric amplitude or the dielectric strength of the relaxation process, α_j and β_j are the symmetric and the asymmetric broadening parameters of the distribution of relaxation times, j in the subscript refers to j^{th} relaxation process. One should note that the WINFIT software uses $\alpha_{(H-N)}$ instead of $(1-\alpha_{Cole-Cole})$ in Eq. (1). The fitting is justified as steps in the real parts of permittivity and broad peaks in the dielectric loss spectra are observed. The experimental data are fitted to the three relaxation processes, i.e. n = 3 to obtain better fit of the experimental data to the H-N equation. Figs. 5 and 6 show just two examples of fitting the real and imaginary parts of the permittivity to three different relaxation processes at a temperature of 90 °C in the N phase. The two broadening distribution parameters are found as: $\alpha_j = 1$ and $\beta_j = 1$, where j = 1, 2 indicative of the Debye type relaxation processes. Temperature dependencies of the fitted relaxation parameters such as the dielectric strengths and the relaxation frequencies are shown in Figs. 7 and 8 for both the homeotropic and the planar-aligned cells, respectively.

The first glance at Figs. 3–8 shows several unusual features in the observed experimental results. Unlike a conventional liquid crystalline nematic phase that normally shows typical molecular relaxation processes, here up to three collective relaxation processes are observed in DIO. These are denoted by P_0, P_1, and P_2 in the order of the increase in the relaxation frequency. P_0 is the lowest frequency process, it arises from the dynamics of ions in the medium having accumulated on the alignment layers under weak electric field. The dielectric strength of P_0 in a homeotropic cell is much higher than in a planar-aligned cell on account of the easier migration of ions that occurs along the molecular director than normal to it. This parasitic, non-molecular pseudo-relaxation process P_0 is out of the current focus and is henceforth excluded from further discussion in this article.

Another remarkable finding of the study is the extremely high dielectric permittivity (Fig. 7), of the order of 3000 in the N_F phase. In general, the cell for dielectric measurements consists of two glass substrates deposited with ITO. Each of the electrodes of the cell is coated with a thin layer of polymer to obtain planar or homeotropic alignment, as the case may be. The polymer layer forms an additional parasitic capacitance connected in series with the LC layer. If the material under investigation has a low to moderate dielectric permittivity value, then the capacitance of the LC layer is much lower than of the polymer itself, the total capacitance of the cell then corresponds to the LC layer itself, for capacitances connected in series. However, some ferroelectric nematics or smectics do possess extremely large spontaneous polarization values. Clark et al. [33] showed that in the absence of an external electric field, the polarization vector **P** in such a case is parallel to the surface of the substrates in a planar-aligned cell. The external field as applied exerts a torque on **P** resulting into its field induced reorientation, this in turn generates a polarization current that transports the charge across the N_F layer. This creates a combined polarisation-capacitance Goldstone (PCG) mode. Due to a large **P** in the N_F, the process occurs in such a manner that the field applied is almost completely screened by the transported polarization charge. The voltage thus applied to the cell appears entirely across the capacitance of the alignment layer and hence the measured cell capacitance is of the alignment layer itself.

In relation to our measurements, a total capacitance of the test cell can be represented by capacitances of the: (i) LC layer (C_{LC}) in series with a combined capacitance of the two polymer alignment layers (C_P). The total (or measured/apparent) capacitance $C_T = \frac{C_{LC} \cdot C_P}{C_{LC} + C_P}$ may have two extreme values: $C_T|_{C_{LC} \gg C_p} = C_p$ and $C_T|_{C_{LC} \ll C_p} = C_{LC}$. Equating $C_{LC} = \frac{\varepsilon_{LC}\varepsilon_0 A}{d_{LC}}$ and $C_P = (\varepsilon_P\varepsilon_0 A)/d_P$, we find that the maximum value of the apparent (or the measured) dielectric permittivity can be obtained from capacitance C_p as $\varepsilon_{LC}^a = \frac{\varepsilon_p d_{LC}}{d_p}$. For d_{LC} = 4 μm, d_p = 40 nm and $\varepsilon_p \approx 5$, the maximum apparent value of the dielectric permittivity $\varepsilon_{LC}^* \approx 500$, where 'a' in the superscript of permittivity denotes its apparent value. It is closer to the experimental value $\varepsilon_{LC}^* \approx 700$, see Fig. 8a for the planar aligned cell. This estimated value is rather approximate due to a possible variation in the cell parameters, especially the thickness of the polymer layer itself. The maximum measured permittivity of the LC in a homeotropic cell, having the same parameters as of the planar aligned cell, is $\varepsilon_\parallel \sim 3000$ [see (Fig. 7(a))]. A comparison between these values may imply that 700 in effect could be the closer to the actual $\varepsilon_\perp$ permittivity of the material, since $\varepsilon_\parallel \gg \varepsilon_\perp$. This conclusion is further supported by measurements in cells with bare ITO electrodes (i.e., ITO substrates without alignment layers), where the parasitic capacitance of the polymer layers is absent. The ITO cell filled with DIO in the absence of alignment layers shows a Schlieren texture under POM. Here the reason for the observed Schlieren texture is that 'the average director **n** of the molecules' is neither parallel nor perpendicular to the electrodes. The maximum value of $\Delta\varepsilon$ measured without alignment layers is found to be ~ 1000 (not shown in plots), a value that lies in between the parallel $\varepsilon_\parallel$ and the perpendicular $\varepsilon_\perp$ permittivity val-
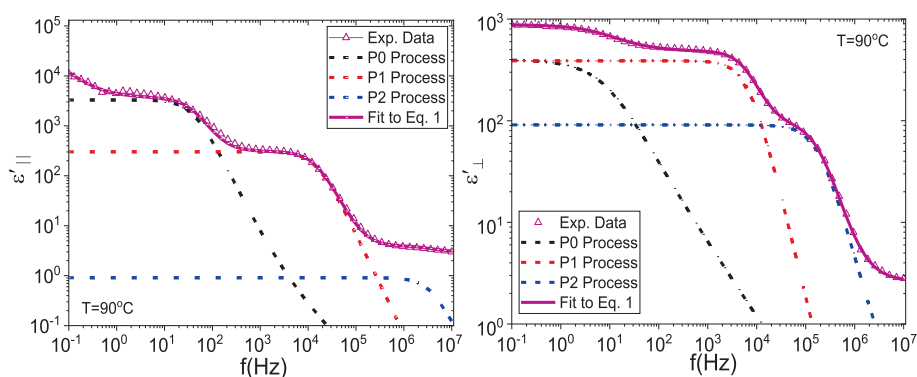
Fig. 5. Frequency (f) dependence of the real part of permittivity at a temperature of 90 °C in the nematic phase. The triangular symbols represent experimental data, the solid magenta line is the fit to Eq. (1), while the black, red, and blue dash lines denote three processes: P_0, P_1 and P_2, respectively for (a) homeotropic and (b) planar alignment. (For interpretation of the references to colour in this figure legend, the reader is referred to the web version of this article.)
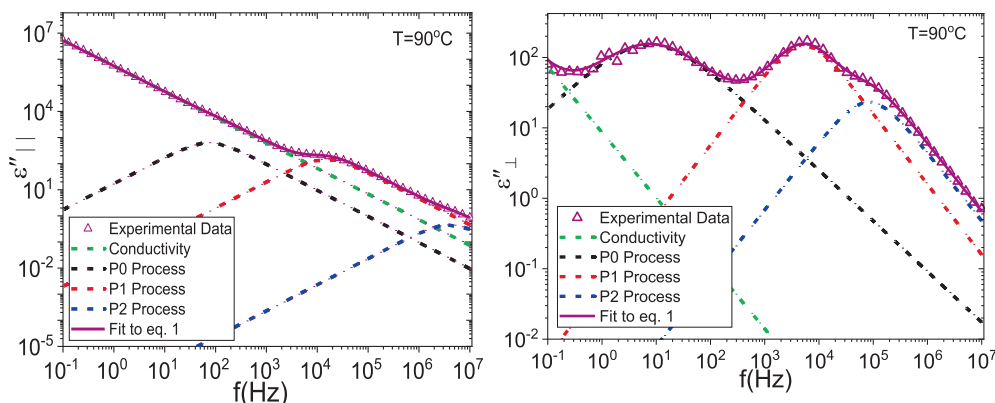
Fig. 6. Frequency (f) dependence of the dielectric loss spectra at a temperature of 90 °C in the nematic phase. The triangular symbols correspond to experimental data, solid magenta line is the fit to Eq. (1), green dash lines each with a slope of −1 on the log–log scale indicate conductivity plots while the black, red, and the blue dash lines denote three processes viz. P_0, P_1 and P_2, respectively for the two alignments (a) homeotropic $\varepsilon_{\parallel}$ and (b) $\varepsilon_{\perp}$ for planar-aligned cell. (For interpretation of the references to colour in this figure legend, the reader is referred to the web version of this article.)
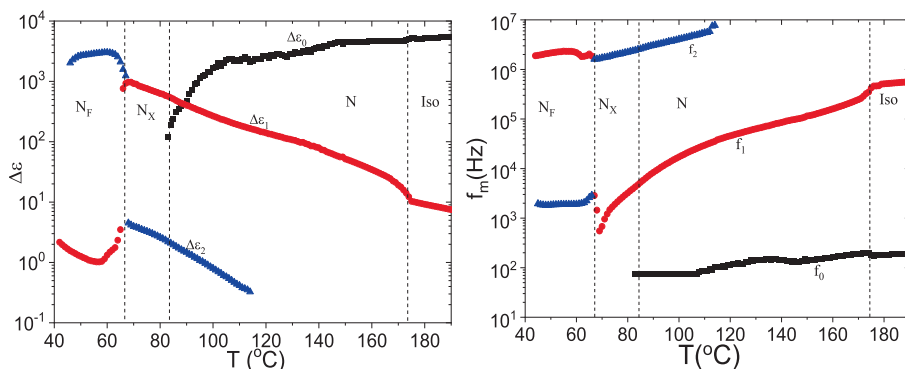
Fig. 7. Temperature dependence of the dielectric relaxation parameters for a homeotropic cell with a sample thickness of 4 μm (a) dielectric strength ($\Delta\varepsilon$) and (b) the relaxation frequency (f_m). The data points are shown in different colors: Black (P_0), Red (P_1) and Blue (P_2). The subscripts: 0, 1 and 2 refer to the modes/processes P_0, P_1 and P_2, respectively. (For interpretation of the references to colour in this figure legend, the reader is referred to the web version of this article.)
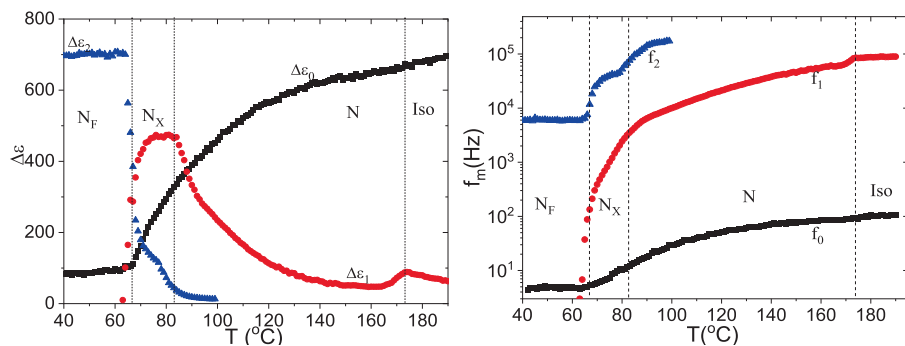
Fig. 8. Temperature dependencies of the relaxation parameters of a planar aligned cell of cell-thickness of 4 μm (a) the dielectric strength ($\Delta\varepsilon$) and (b) the relaxation frequency (f_m). The data points shown in various colors refer to: Black (P_0), Red (P_1) and Blue (P_2). (For interpretation of the references to colour in this figure legend, the reader is referred to the web version of this article.)

ues. However, precise configuration of the liquid crystalline molecules in cells without alignment layers is ambiguous and therefore the measured value of permittivity cannot be assigned to either $\varepsilon_{\parallel}$ or $\varepsilon_{\perp}$. Molecules are aligned only in the LC cells having proper alignment layers on the opposite facing substrates: homeotropic or planar as is confirmed by the textures recorded under POM in situ of the dielectric experiment.

In this article, we primarily focus on to studying the N and the N_X phases in which the dielectric permittivity is relatively low, compared to that of the N_F phase, and where the parasitic capacitance of the alignment layers can be neglected as the total capacitance of capacitors of unequal values connected in series equals the least capacitance, if it is much lower than the other capacitance in the circuit. For cells with alignment layers on the electrodes, in addition to P_0, two additional collective relaxation processes are observed in the N and N_X phases of DIO. The physical origin of each of these two processes is discussed below:

The mechanism/origin of the process P_1: Temperature dependencies of the dielectric parameters of the mid-frequency relaxation process P_1 are shown as $\varepsilon_\parallel$ in Fig. 7a and, $\varepsilon_\perp$ in Fig. 8a in terms of dielectric strengths. P_1 is present in the entire range of temperatures of the N and N_X phases. The average value of the permittivity at the isotropic to nematic phase transition is given by the formula, $\varepsilon_{iso} = (\varepsilon_\parallel +2\varepsilon_\perp)/3$ aʳ Hence, on the phase transition from the isotropic (Iso) to the N phase, the dielectric strength should increase to $\varepsilon_\parallel$ in a homeotropic cell and reduce to $\varepsilon_\perp$ in a planar aligned cell. The results are are shown in Fig. 7a and 8a, respectively, which determine the mechanism of P_1 as follows: in the isotropic phase P_1 corresponds to the flip flop rotation of the individual molecules around their short axes in agreement with a conclusion drawn in [12], where the dipole fluctuations are related to the collective molecular rotation about their short axes. In general, this mode should also exist in the N phase. In addition, the temperature dependence of the relaxation frequency of the molecular relaxation process should follow the Arrhenius behavior, $f_m(T) = Ae^{\frac{-E_a}{RT}}$, where E_a is the activation energy. A plot of log $f_m(T)$ versus $1/T$ should have been a straight line, though not observed here. Instead, the temperature dependence of the frequency of this mode shows a soft mode - like critical behavior, observed for the first time in a ferronematic phase, i.e., the relaxation frequency is observed to decrease linearly from the N phase with a reduction in temperature to the N_X-N_F phase transition temperature. A softening of the splay elastic constant for RM734 has been observed in ref.[9]. On the transition to the nematic phase, the process involves relaxation dynamics of molecules with short-range correlations. On further cooling of the sample, the correlation length (and the volume of domains) continues to grow in the N and the N_X phases, the relaxation frequency of P_1 decreases with a reduction in temperature as $\sim (T-T_{NX})$. Thus, P_1 exhibits soft mode – like characteristic behavior with a critical temperature corresponding to the N_X-N_F transition temperature. This is one of the major characteristic features of the second–order like phase transition. Surprisingly, the dielectric strength does not follow the soft mode characteristic in the N_X phase, it initially saturates and then decreases on cooling in the N_F. This inconsistency has a simple explanation. The maximum dielectric strength is limited by the capacitance of the alignment layers, as $\Delta\varepsilon_1 + \Delta\varepsilon_2 < 700$ and the apparent value of $\Delta\varepsilon_1$ drops due to a faster growth in $\Delta\varepsilon_2$.

It is important to mention here that the other ferronematic compound RM734 and its homologous show only one collective relaxation process in the paraelectric nematic phase [12], similar to the behavior of the mode P_1 (Figs. 7 and 8 in red) i.e. (i) P_1 in RM734 lies in a similar frequency range; (ii) it shows soft mode-like temperature dependence on transition to the ferronematic phase; (iii) it exists in both phases: isotropic and the paraelectric nematic; (iv) it is detected at frequencies lower than those in the Iso phase. Therefore, we can assign P_1 to the collective mode, similar to that observed in RM734, attributed to "amplitude mode", describing the collective dynamics of dipoles [12]. These dipoles are strongly coupled to the splay fluctuations of the groups of molecules and this coupling of dipoles with splay promotes a growth in the polarization.

The mechanism/origin of P_2: In general, the temperature dependencies of the dielectric parameters of the high–frequency relaxation process P_2 appear like the relaxation process P_1. However, P_2, does not exist in the isotropic phase, it emerges only in the nematic phase at ~ 110 °C. This mode may possibly exist at higher temperatures, starting presumably from the Iso - N phase transition temperature, but in practice it is too weak to be unambiguously observed. This may mean that in the paraelectric nematic phase, polar domains with limited correlation lengths of the dipoles do exist in the medium, the size of the domains increases

under cooling and finally in the N_F phase, the dipoles collectively undergo dynamics as in ferroelectric phason (or Goldstone) mode. P_2 shows the soft mode like characteristic behavior for both phase transition temperatures, N - N_X and N_X - N_F. This mode could have easily been assigned to the amplitude "ferroelectric mode" P_1 but with having a different physical mechanism. This mode is not observed in RM734 series of compounds. Hence DIO must have an additional characteristic feature that yields P_2. This feature is observed from POM studies of the material discussed in detail in Ref. [34]. Here, the observed textures of a planar aligned cell with parallel rubbed surfaces are homogeneously uniform. However, in cells fabricated using one substrate with a rubbed surface, and the second with a non-rubbed surface, the texture exhibits chiral domains of opposite chirality emerging at a temperature just below the Iso-N phase transition temperature. Under such conditions, the position of the director is fixed along the rubbing direction on rubbed surface, whereas it moves around on the unrubbed surface as it is degenerate, i.e., the arrangement of directors follows the natural activity of the material in the bulk. Chiral domains arise from the segregation of DIO molecules of the opposite chirality. Such a segregation arises from the chiral symmetry breaking and is also observed in the isotropic phase by Tschierske et al. [35] though the medium there is that of percolated liquids with a network structure. The spontaneous polarization and the polarity are usually related to the optical activity as in Ferroelectric LCs. Furthermore, a recent study [36] shows that DIO when doped with an optically active dopant (OAD) leads to a new polar cholesteric phase denoted by N_P^*. In this doped system, a collective mode is observed in the paraelectric cholesteric phase, where it shows soft mode like characteristic behavior on approaching the transition temperature to the polar N_P^* phase, as is observed in pure achiral DIO. In the former case, the chiral dopant is the explicit prerequisite for the emergence of ferroelectricity whereas in achiral DIO, it arises implicitly from the segregated molecules of opposite chirality that lie in domains of the opposite optical activity. However, the optical textures of RM734 and its homologues, using cells of similar geometry as for DIO, show perfect homogenous alignment with no sign of optical activity present in the high temperature N phase. Hence, here the spontaneous symmetry breaking is the exclusive property of DIO, this has not yet been reported in other ferronematic compound/s.

At the phase transition temperature, I - N, the chiral molecules of opposite chirality start segregating from each other and form chiral domains each, with the conformers of opposite sense of helicity. Conformers of the same sense helicity are favored to form a densely packed structure than the packing together of the two types of molecules in the condensed phase arising from a reduced excluded volume. The correlation lengths of these domains grows under cooling, and finally the domain of a 'single chirality' occupies the entire volume of the cell close to the transition temperature to the ferroelectric nematic phase. Hence, in addition to the amplitude mode arising from the process P_1, we have an additional collective process P_2 that arises from the dynamics of the chiral segregated molecules.

Process P_2 is examined in greater detail to ensure that its relaxation parameters: the peak frequency and the dielectric strength, are not affected by the ITO peak. We performed dielectric measurements on the LC cells using substrates with two sheet resistances: a low 10 $\Omega/\square$ and a high ITO sheet resistances of 100 $\Omega/\square$. We estimate the frequency of the parasitic ITO process for cells used with the parameters: area of electrodes $A = 0.18$ cm^2; cell spacing = 4 μm. For the empty cell, the cut-off frequency of the parasitic ITO peak is ~ 40 MHz and for the filled cells with $\varepsilon_{rel} \approx 5$, the cut-off frequency $f_{ITO} \approx 8$ MHz.. However, for $R = 10$ $\Omega/\square$ cells, $f_{ITO} \approx 80$ MHz, that lies well beyond the frequency window of the
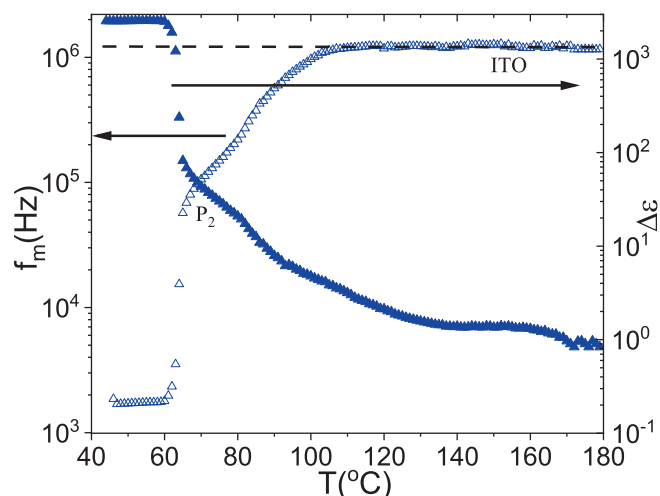
Fig. 9. The temperature dependencies of the dielectric strength $\Delta\varepsilon$ and the relaxation frequency f_m plotted both on the log–log scale in the ordinates as a function of temperature for the P_2 mode using a LC cell with the two substrates, each having a sheet resistance of 100 $\Omega/\square$.

experiment. To confirm it, we measured the dielectric spectra in the 100 $\Omega/\square$ cell. The plot of dielectric parameters in Fig. 9 shows the temperature dependencies of the highest frequency peak and dielectric strength of this mode. This curve now arises from a combination of the relaxation process P_2 and the parasitic ITO peak.

For higher temperatures in the range 110–175 °C, this peak is temperature independent as expected for the parasitic ITO mode. However, below a temperature of ~105 °C, the dielectric strength $\Delta\varepsilon$ increases dramatically on cooling and hence the parameters shown are dominated by the relaxation process P_2. This is clearly observed in the cells with a sheet resistance of 10 $\Omega/\square$ (see Figs. 5–7). This may also explain as to why the mode observed by Brown et al. [20] is seen only in the N_X phase, where the dielectric strength is much greater than for higher temperatures. However, for the cells fabricated with a low resistance ITO substrates, 10 $\Omega/\square$, P_2 is not affected by the ITO peak and is observed unambiguously even in the high temperature paraelectric nematic phase, N. Measurements of the real and the imaginary parts of permittivity are plotted in Supplemental Fig. 1 in the frequency range 1 Hz–10 MHz of an empty cell, with the sheet resistance of 10 $\Omega/\square$. In the experimental frequency range 1 Hz–10 MHz, ITO peak is beyond the frequency of 10 MHz.

4. Conclusions

Summarizing, three relaxation processes are observed experimentally in the dielectric spectra of DIO. The least-frequency relaxation process P_0 is assigned to the dynamics of ions from the accumulation of the charge on the alignment layers. The mid-frequency P_1 starts off as the collective orientation of the molecular dipoles around their short axes (the flip-flop mode) in the isotropic phase. On entering the paraelectric nematic phase from the Iso phase, dipoles are coupled strongly with the splay fluctuations [9,12,20]. P_1 demonstrates a soft mode like behavior on approaching the ferronematic phase and is the amplitude mode. The high-frequency P_2 originates from the dynamics of chiral segregated molecules in polar/chiral domains originating from the spontaneous symmetry breaking of achiral mesogens of DIO. Both collective processes, P_1 and P_2 contribute to the formation of the ferronematic phase. The mechanism for the formation of the ferronematic phase in DIO is found to be different to that in RM734.

Data availability

Data will be made available on request.

Declaration of Competing Interest

The authors declare that they have no known competing interests or personel relationships that might have appeared to influence the work reported in this paper.

Appendix A. Supplementary material

Supplementary data to this article can be found online at https://doi.org/10.1016/j.molliq.2023.121570.

References

[1] T. Niori, T. Sekine, J. Watanabe, T. Furukawa, H. Takezoe, Distinct ferroelectric smectic liquid crystals consisting of banana shaped achiral molecules, J. Mater. Chem. 6 (1996) 1231, https://doi.org/10.1039/JM9960601231.

[2] V.P. Panov, M. Nagaraj, J.K. Vij, Y.P. Panarin, A. Kohlmeier, M.G. Tamba, R.A. Lewis, G.H. Mehl, Phys. Rev. Lett. 105 (2010), https://doi.org/10.1103/PhysRevLett.105.167801.

[3] V.P. Panov, R. Balachandran, M. Nagaraj, J.K. Vij, M.G. Tamba, A. Kohlmeier, G.H. Mehl, Microsecond linear optical response in an unusual nematic phase of achiral bimesogens, Appl. Phys. Lett. 99 (2011), https://doi.org/10.1063/1.3671996.

[4] P. Debye, Einige Resultate einer kinetischen Theorie der Isolatoren, Physik. Z 13 (1912) 97.

[5] M. Born, Elektronentheorie des natürlichen optischen Drehungsvermögens isotroper und anisotroper Flüssigkeiten, Ann. Phys. 360 (1918) 177–240, https://doi.org/10.1002/andp.19183600302.

[6] H. Nishikawa, K. Shiroshita, H. Higuchi, Y. Okumura, Y. Haseba, S. Yamamoto, K. Sago, H. Kikuchi, A fluid liquid-crystal material with highly polar order, Adv. Mater. 29 (2017) 1702354, https://doi.org/10.1002/adma.202101305.

[7] R.J. Mandle, S.J. Cowling, J.W. Goodby, Rational design of rod-like liquid crystals exhibiting two nematic phases, Chem. Eur. J. 23 (2017) 14554, https://doi.org/10.1002/chem.201702742.

[8] X. Chen, V. Martinez, E. Korblova, G. Freychet, M. Zhernenkov, M.A. Glaser, C. Wang, C. Zhu, L. Radzihovsky, J.E. Maclennan, D.M. Walba, N.A. Clark, The smectic Z_A phase: Antiferroelectric Smectic Order as a prelude to the Ferroelectric nematic, PNAS 120 (2023) e2217150120., https://doi.org/10.1073/pnas.2217150120.

[9] N. Sebastián, M. Copic, A. Mertelj, Phys. Rev. E 106 (2022), https://doi.org/10.1103/PhysRevE.106.021001.

[10] R. Mandle, S. Cowling, J.W. Goodby, A nematic to nematic transformation exhibited by a rod-like liquid crystal, Phys. Chem. Chem. Phys. 19 (2017) 11429, https://doi.org/10.1039/C7CP00456G.

[11] A. Mertelj, L. Cmok, N. Sebastián, R.J. Mandle, R.R. Parker, A.C. Whitwood, J.W. Goodby, M. Čopič, Splay Nematic Phase, Phys. Rev. X 8 (2018), https://doi.org/10.1103/PhysRevX.8.041025.

[12] N. Sebastián, L. Cmok, R.J. Mandle, M. Rosario de la Fuente, I. Drevenšek Olenik, M. Čopič, A. Mertel, Ferroelectric-ferroelastic phase transition in a nematic liquid crystal, Phys. Rev. Lett.. 124 (2020), https://doi.org/10.1103/PhysRevLett.124.037801.

[13] R.J. Mandle, S.J. Cowling, J.W. Goodby, Structural variants of RM734 in the design of splay nematic materials, Liq. Cryst. 48 (2021) 1780, https://doi.org/10.1080/02678292.2021.1934740.

[14] R. J. Mandle, N. Sebastián, J. Martinez-Perdiguero, A. Mertelj, On the molecular origins of the ferroelectric splay nematic phase, Nat. Commun. 12 (2021) 4962, https://doi.org/10.1038/s41467-021-25231-0.

[15] X. Chen, E. Korblova, D. Dong, X. Wei, R. Shao, L. Radzihovsky, M.A. Glaser, J.E. Maclennan, D. Bedrov, D.M. Walba, N.A. Clark, First-principles experimental demonstration of ferroelectricity in a thermotropic nematic liquid crystal: Polar domains and striking electrooptics, PNAS. 117 (2020) 14021–14031, https://doi.org/10.1073/pnas.2002290117.

[16] X. H. Zhao, J. C. Zhou, J. X. Li, J. Kougo, Z. Wan, M. J. Huang and S. Aya, Spontaneous helielectric nematic liquid crystals: electric analog to helimagnets, Proc. Natl. Acad. Sci. U.S.A. 118 (2021) e2111101118, doi: 10.1073/pnas.2111101118.

[17] A. Manabe, M. Bremer, M. Kraska, Ferroelectric nematic phase at and below room temperature, Liq. Cryst. 48 (2021) 1079, https://doi.org/10.1080/02678292.2021.1921867.

[18] R. Saha, P. Nepal, C. Feng, M.S. Hossein, M. Fukuto, R. Li, J.T. Gleeson, S. Sprunt, R.J. Twieg, A. Jákli, Multiple ferroelectric nematic phases of a highly polar liquid crystal Compound, Liq. Cryst. (2022), https://doi.org/10.1080/02678292.2022.2069297.

[19] D. Pociecha, R. Walker, E. Cruickshank, J. Szydlowska, P. Rybak, A. Makal, J. Matraszek, J.M. Wolska, J.M.D. Storey, C.T. Imrie and E. Gorecka, Intrinsically chiral ferronematic liquid crystals, arXiv:2112.11887 [Cond-mat.soft] (2021).

[20] S. Brown, E. Cruickshank, J.M.D. Storey, C.T. Imrie, D. Pociecha, M. Majewska, A. Makal, E. Gorecka, Multiple polar and non-polar nematic phases, Chem. Phys. Chem. 22 (2021) 2506, https://doi.org/10.1002/cphc.202100644.

[21] Y.P. Panarin, H. Xu, S.T. MacLughadha, J.K. Vij, Dielectric Response of Ferroelectric Liquid Crystal Cells, Jpn. J. Appl. Phys.. 33 (1994) 2648, https://doi.org/10.1143/JJAP.33.2648.

[22] H. Xu, Y.P. Panarin, J.K. Vij, A.J. Seed, M. Hird, J.W. Goodby, Investigation of the TGBA* phase in a ferroelectric liquid crystal using dielectric spectroscopy, J. Phys. Condens. Matter 7 (1995) 7443, https://doi.org/10.1088/0953-8984/7/38/004.

[23] Y.P. Panarin, H. Xu, S.T. MacLughadha, J.K. Vij, A.J. Seed, M. Hird, J.W. Goodby, An investigation of the field-induced ferrielectric subphases in antiferroelectric liquid crystals, J. Phys. Condens. Matter. 7 (1995) L351, https://doi.org/10.1088/0953-8984/7/27/001.

[24] Y.P. Panarin, O.E. Kalinovskaya, J.K. Vij, J.W. Goodby, Observation and investigation of the ferrielectric subphase with high q_T parameter, Phys. Rev. E 55 (1997) 4345, https://doi.org/10.1103/PhysRevE.55.4345.

[25] Y.P. Panarin, O.E. Kalinovskaya, J.K. Vij, The investigation of the relaxation processes in antiferroelectric liquid crystals by broad band dielectric and electro-optic spectroscopy, Liq. Cryst. 25 (1998) 241, https://doi.org/10.1080/026782998206399.

[26] N. Yadav, V.P. Panov, V. Swaminathan, S.P. Sreenilayam, J.K. Vij, T.S. Perova, R. Dhar, A. Panov, D. Rodriguez-Lojo, P.J. Stevenson, Chiral smectic-A and smectic-C phases with de Vries characteristics, Phys. Rev. E 95 (2017), https://doi.org/10.1103/PhysRevE.95.062704.

[27] S. Sreenilayam, Y.u. Panarin, J.K. Vij, Dielectric study of nematic LC built with bent-core molecules, Mol. Cryst. Liq. Cryst. 610 (2015) 63, https://doi.org/10.1080/15421406.2015.1025207.

[28] N. Yadav, R. Dhar, in: D.K. Singh, M. Pradhan (Eds.), Impedance spectroscopy in modern techniques of spectroscopy: basics, instrumentation and applications, Springer, 2021, pp. 515–540.

[29] S. Sreenilayam, Y.P. Panarin, J.K. Vij, A. Lehmann, M. Poppe, C. Tschierske, Development of ferroelectricity in the smectic phases of 4-cyanoresorcinol derived achiral bent-core liquid crystals with long terminal alkyl chains, Phys. Rev. Materials 1 (2017), https://doi.org/10.1103/PhysRevMaterials.1.035604.

[30] S. Havriliak, S. Negami, A complex plane analysis of α-dispersion in some polymer systems, J. Polym. Sci. C 14 (1966) 99, https://doi.org/10.1002/polc.5070140111.

[31] F. Kremer, S.U. Vallerien, R. Zentel, H. Kapitza, Broad-Band Dielectric Spectroscopy on a Set of Combined Main-Chain Side-Group Liquid-Crystalline Polymers, Macromolecules 22 (1989) 4040–4045, doi: 10.1021/ma00200a037.

[32] R. Dhar, Comments on the fitting of Cole-Cole/Havriliak–Negami equation with the dielectric data under the influence of parasitic effects in order to extract correct parameters of the materials, J. Mol. Liq. 343 (2021) 117682, https://doi.org/10.1016/j.molliq.2021.117682.

[33] N.A. Clark, Xi Chen, J.E. Maclennan, M.A. Glaser, Dielectric spectroscopy of ferroelectric nematic liquid crystals: measuring the capacitance of insulating interfacial layers, arXiv:2208.09784 (2022).

[34] N. Yadav, Y.P. Panarin, W. Jiang, G.H. Mehl, J.K. Vij, Spontaneous mirror symmetry breaking and chiral segregation in an achiral ferronematic compound DIO, Phys. Chem. Chem. Phys. (2023), https://doi.org/10.1039/D3CP00357D.

[35] C. Dressel, T. Reppe, M. Prehm, M. Brautzsch, C. Tschierske, Chiral self-sorting and amplification in isotropic liquids of achiral molecules, Nat. Chem. 6 (2014) 971, https://doi.org/10.1038/nchem.2039.

[36] H. Nishikawa, F. Araoka, A New Class of Chiral Nematic Phase with Helical Polar Order, Adv. Mater. 2021 (2021) 2101305, https://doi.org/10.1002/adma.202101305.

[37] B.K.P. Scaife, Principles of Dielectrics, Oxford University Press, London (1989), revised edition 1998.

[38] V.P.Panov, R. Balachandran, J. K. Vij, M. G. Tamba, A. Kohlmeier, G. H. Mehl, Field induced periodic chiral pattern in the N_X phase of achiral mesogens,Appl. Phys. Lett. 101 (2012) 234106. doi: 10.1063/1.4769458.